Contributions to Mineralogy and Petrology (2026) 181:2
https://doi.org/10.1007/s00410-025-02288-4

ORIGINAL PAPER

Impurity poisoning as a mechanism for the formation of zircon oscillatory growth zones

Marisa D. Acosta[1] · James M. Watkins[2] · Denis Fougerouse[3] · Michelle L. Foley[4] · Oliver Plümper[5] · David W. Saxey[6] · Steven M. Reddy[3] · Mark H. Reed[7]

Received: 1 July 2025 / Accepted: 8 December 2025

Abstract
Oscillatory zoning — alternating high- and low-impurity (trace element) zones — is a hallmark of magmatic zircon from felsic systems and preserves the history of magmatic systems. Although commonly attributed to fluctuations in temperature, pressure, or melt composition, the mechanisms driving this zoning remain uncertain. Here, we show that high-impurity growth zones, which appear homogeneous when imaged with a scanning electron microscope (SEM), actually consist of finer-scale growth zones when viewed at the nanoscale - and still finer zones are revealed at the atomic scale. The apparent homogeneity in SEM images results from electron beam convolution, where features smaller than the beam's interaction volume cannot be resolved. Backscattered electron images have higher spatial resolution than cathodoluminescent images, but high-impurity zones imaged with both are found to consist of finer zones at the atomic scale when imaged with atom probe tomography. Adjacent low-impurity zones are homogeneous across all scales. We interpret these observations as evidence of impurity poisoning during near-equilibrium zircon growth. Faceted crystal growth at low supersaturation leads to rejection of impurities, except for those allowed by equilibrium partitioning. Rejected impurities accumulate on the crystal surface, blocking normal incorporation of atoms and temporarily halting growth. When supersaturation exceeds a critical threshold, growth resumes, trapping the adsorbed impurities and forming a high-impurity zone. These findings not only help to resolve the origin of oscillatory zoning in zircon but also establish a generalizable mechanism of impurity poisoning during near-equilibrium crystal growth, redefining how mineral records are interpreted in igneous systems and beyond.

Keywords Zircon · Oscillatory zoning · Impurity poisoning · Dead zone

Introduction

A striking feature of magmatic zircon from felsic systems is that it commonly exhibits trace element oscillatory zoning. While this zonation is broadly understood to reflect changes in growth conditions, the origin and significance of growth zoning remains a topic of debate, as detailed in the text below. The texture, which consists of alternating, micron-scale layers of high-impurity and low-impurity growth zones, also occurs in many other minerals precipitated from

Communicated by Ralf Dohmen.

✉ Marisa D. Acosta
mdacosta@alaska.edu

[1] The Geophysical Institute & Department of Geosciences , University of Alaska Fairbanks, Fairbanks, USA

[2] Department of Earth and Physical Sciences, University of California-Davis, Davis, USA

[3] School of Earth and Planetary Sciences, Curtin University, Perth, Australia

[4] Department of Geosciences, University of Arizona, Tucson, USA

[5] Faculty of Geosciences (FB05) & MARUM, Center for Marine Environmental Sciences, University of Bremen, Bremen, Germany

[6] Geoscience Atom Probe, John de Laeter Centre, Curtin University, Perth, Australia

[7] Department of Earth Sciences, University of Oregon, Eugene, USA

Published online: 03 January 2026

a fluid medium. For example, oscillatory growth zoning is commonly reported in hydrothermal quartz (Acosta et al. 2022), hydrothermal calcite (Barker and Cox 2011), diamonds from the mantle (Wiggers de Vries et al. 2013), and garnets in subduction zone mélanges (George et al. 2024). This suggests a common mechanism influences oscillatory growth zone formation in many mineral-fluid systems.

At thermodynamic equilibrium, trace element variations within zircon record fluctuations in temperature, pressure, or local composition of the growth medium. However, in many cases, the large magnitude of trace element variations (100's – 1000's of ppm) precludes equilibrium partitioning (Hofmann et al. 2009; Yang et al. 2016; Acosta et al. 2022). This has led to speculation that oscillatory zoning may arise from kinetic feedback at the crystal/melt interface (e.g., Hoskin and Schaltegger 2003; Hofmann et al. 2009), but it remains a challenge to interrogate these processes as they take place at the nanometer scale.

In this contribution, we emphasize that SEM imaging cannot resolve the smallest growth zones because of beam convolution. We show that CL-dark/BSE-bright zones are self-affine to the scale of interplanar d-spacing; these apparently homogeneous growth zones imaged with SEM are in fact made of smaller and finer zones at higher-resolution. Adjacent CL-bright/BSE-dark zones are homogeneous at all investigated resolutions. We suggest that impurity poisoning is a simple and elegant explanation for these observations, which are difficult to reconcile with other growth mechanisms. Impurity poisoning is a crystal growth phenomenon that can be understood within the terrace-ledge-kink theoretical framework – a framework that encompasses several observations made in this dataset: particularly that as growth zones are imaged from the microscale to nanoscale to atomic-scale resolution, progressively finer zoning is revealed, and that across all scales growth zones should be integer multiples of d-spacings for a given face with atomically sharp boundaries between them. We review this framework in depth situating our novel observations within the existing canon of crystal growth literature. We emphasize that oscillatory zoning is an expected outcome of near-equilibrium crystal growth at low degrees of supersaturation. This general model may apply to all faceted crystals with trace element oscillatory growth zones.

Characteristics of zircon oscillatory growth zones

Zircon growth zones typically display alternating patterns of relative trace element enrichment and depletion, mostly involving high-field-strength elements (Hf, Ti, Nb, Ta), rare earth elements, and U, Th, Y, P. We distinguish between high-impurity zones and low-impurity zones. High-impurity zones contain hundreds to thousands of ppm of trace elements, whereas low-impurity zones contain only tens to hundreds of ppm. We assume that most of the impurities/trace elements in zircon have heavier atomic numbers than Zr-Si-O so that the high-impurity zones have higher mean atomic numbers. In high-impurity zones, trace element concentrations can range from hundreds to thousands of ppm (Hoskin and Schaltegger 2003; Corfu et al. 2003). Cathodoluminescent-visible zone thicknesses range from approximately 1 to 100 microns (Halden and Hawthorne 1993; Corfu et al. 2003), but the lower end of this scale is close to the resolution limit of SEM-CL.

Superimposed on these fine-scale zones are commonly broader-scaled trends of trace element enrichment or depletion that extend from crystal cores to rims (Shore and Fowler 1996). This signal is separate from that recorded in oscillatory growth zones and likely reflects gradual changes in melt composition and temperature as the melt evolves.

Advances in analytical techniques have enabled increasingly detailed characterizations of zircon zoning. SEM-CL can resolve zonations down to the micron-scale (Halden and Hawthorne 1993; Hoskin 2000). NanoSIMS and TOF-SIMS measurements extended this resolution to the submicron scale (Hofmann et al. 2009; Yang et al. 2016), and atom probe tomography (APT) studies have identified nanoscale trace element features (Valley et al. 2014; Peterman et al. 2016) and atomically sharp interfaces (Reddy et al. 2016; Piazolo et al. 2016; Peterman et al. 2019; Foley et al. 2024). The small scale of enriched zones with atomically sharp boundaries challenge models of zircon growth that invoke local equilibrium at the crystal-melt interface and/or rely on continuum approximations of melt structure and diffusion (e.g., L'Heureux, 1993; L'Heureux & Fowler, 1996; Watson 1996; Hoskin 2000; Melnik and Bindeman 2018) because such models predict diffuse boundaries at the atomic scale. Exclusively diffusion-driven mechanisms for oscillatory growth cannot explain the observation of atomically sharp, planar interfaces.

Types of oscillatory growth zoning

There are two categories of oscillatory growth zoning that are evaluated further in the following sections: extrinsic zones that result from changes in pressure, temperature, or bulk system composition, and intrinsic zones that form by the interplay between element diffusion and surface kinetic processes at the crystal-fluid interface (Shore and Fowler 1996; Wu et al. 2019). Local diffusion usually plays a role in both extrinsic and intrinsic models. Probably these two types of signals are commonly superimposed in zircon because although individual oscillatory zone patterns cannot be traced from one co-genetic crystal to another, fractal statistics reveal large-scale harmonic zone signals that do

correlate from one crystal to the next (Fowler et al. 2002; Holten et al. 1997; Hoskin 2000). Fractal statistics have also been used to quantify the antipersistence of oscillatory zoning, i.e., that the crystal growth surface first accepts and then rejects CL-active impurities (Hanchar et al. 2001; Remond et al. 1992), because of the highly variable trace element concentrations.

We mostly limit the discourse to trace element oscillatory zoning because the processes that form solid solution oscillatory growth zoning are likely different than those that form trace element oscillatory zoning (Pina et al. 2004). Many models of oscillatory growth are focused on solid-solution oscillatory growth (albite-anorthite: L'Heureux and Fowler 1996; L'Heureux and Jamtveit 2002; barite-celestine: L'Heureux and Katsev 2006; Putnis et al. 1992) and may or may not be directly applicable to impurity oscillations. Zircon has a near-ideal solid solution with hafnon, but hafnon concentrations tend to gradually increase from core-to-rim (Claiborne et al. 2010; Carley et al. 2011), reflecting crystal fractionation.

Extrinsic oscillatory growth

Extrinsic models call on fluctuations in fluid composition (due to magma mixing, assimilation of country rock, or more localized composition changes caused by the crystallization of nearby minerals) or pressure and/or temperature to drive changes in trace element partitioning, growth rates, and elemental diffusivities. Melnik and Bindeman (2018) modeled diffusion-controlled zircon growth in spherical coordinates with moving boundary conditions. Their model accounts for diffusion-controlled accessory mineral growth and simultaneous growth of major phases to simulate the influence of temperature- and water- dependent diffusion rates. The model allows for temperature oscillations and varied cooling paths. Melnik and Bindeman (2018) were able to recreate many of the features observed in natural zircon, notably: (1) coeval oscillations of different elements with similar wavelengths but different amplitudes, i.e., the oscillations are between high-impurity and low-impurity growth zones and different elements have different concentrations in the high-impurity growth zones that do not appear to be coupled systematically, (2) wider oscillatory growth zones in crystal cores and narrower zones in rims (Claiborne et al. 2017), (3) oscillatory zoned zircon being a more common texture in grains crystallized from near-solidus, hydrous magma than zircon crystallized from hotter, drier magmas (Carley et al. 2011; Claiborne et al. 2010; Loewen and Bindeman 2016), and (4) core-to-rim increases or decreases in Hf, U, Th, and P because of changes in partitioning and diffusivity during heating or cooling. They conclude that zircon oscillatory zoning cannot be produced by monotonic cooling or crystallization of other minerals alone but that small fluctuations in either temperature or water pressure are necessary because they cause growth rate to vary by modifying element partitioning and diffusivity. Their model captured zone widths from 1 to 10 μm and impurity enrichments that varied by a factor of two between low impurity and high impurity zones.

Intrinsic mechanisms

The large variation in trace element concentration from one zone to the next has led many researchers to conclude that mineral surface disequilibrium kinetics must be responsible for the formation of oscillatory growth. Most quantitative intrinsic models are focused on plagioclase solid solution oscillatory zoning and have been called on to also explain trace element oscillatory zoning; we again note that solid solution oscillatory zoning may not form by the same mechanisms whereby trace element oscillatory zoning does. Allègre et al. (1981) developed a mathematical model for plagioclase growth oscillations. In this model, sinusoidal oscillatory growth zoning forms when the rate of crystal growth is tightly coupled to the rate at which elements are diffusing through the adjacent melt boundary layer. The coupling produces periodic instabilities because as one element (e.g., Ca^{+2}) is preferentially incorporated into the crystal it depletes the adjacent melt in that element. Elements that are not as preferentially incorporated into the crystal gradually build up at the interface. Eventually, composition of the melt in the boundary layer becomes very different from the bulk melt and the growing crystal composition changes to reflect this. L'Heureux (1993) developed the isothermal constitutional undercooling model to explain plagioclase oscillatory growth. In this model, supersaturation changes driven by the coupling between element partitioning during crystal growth and diffusion to or away from the growth interface. Generally, models call on feedback between crystal growth, melt polymerization at the interface, and elemental diffusion across a boundary layer that is between 10 and 100 μm thick (Hoskin 2000). Elements that are rejected from the crystal become enriched at the interface and in the boundary layer, and oscillatory growth zoning is ascribed to the interplay of temperature and element diffusivity and growth rate/supersaturation.

Watson (1996) developed the surface enrichment model to explain disequilibrium trace element enrichments oscillatory and sector zoning. The surface enrichment model emphasizes that impurity uptake during mineral growth depends on the distribution of adsorption sites at the growth surface. Impurities accumulate at the melt–crystal interface when adsorption exceeds desorption and may become incorporated into the crystal during subsequent growth.

Impurity poisoning as the intrinsic mechanism for oscillatory growth zoning

Euhedral oscillatory growth zones preserve a record of faceted crystal growth. Faceted crystal growth mechanisms are readily explained within the framework of terrace-ledge-kink (TLK) theory. Here, we briefly review terrace-ledge-kink theory to emphasize that oscillatory growth is an expected outcome of near-equilibrium crystal growth in impure systems.

The terrace-ledge-kink (TLK) model (Burton et al. 1951) is a generally accepted framework for crystal growth that envisions the topography of a crystal surface as being composed of terraces, ledges, islands, adatoms, and vacancies (Chernov 1961, 1984; De Yoreo and Vekilov 2003). Faceted crystals grow by the lateral advance of step edges through the attachment of solute atoms to kink sites, which implies that the rate of crystal growth scales with the kink site density, or surface roughness (De Yoreo and Vekilov 2003). This general picture is supported by atomic force microscopy imaging, which has been used to measure the advancement rate of step edges and average terrace width of minerals grown from aqueous solution but not silicate melt.

It is well established that impurity atoms can slow crystal growth by blocking kink sites (De Yoreo and Vekilov 2003) and arresting the advancement of steps. Step pinning by impurities can lead to step bunching, where steps become closely spaced, advance as a train, and ultimately merge into a macrostep whose height is an integer multiple of the microstep height. In some systems, macrosteps converge with other macrosteps to form supersteps, which can be 100 microsteps in height or greater.

Other crystal growth mechanisms and models that have been called on to explain oscillatory growth zoning models invariably call on an adhesive growth mechanism. During adhesive growth, atomically rough crystal growth surfaces consist primarily of kink sites so that elements are readily incorporated into the growing crystal. Adhesive growth, also called continuous or rough growth, occurs where the growth surface has a high density of kink sites so that atoms or molecules can attach to the crystal surface at any location. It does not require surface diffusion across atomically smooth terraces to ledges where favorable attachment sites exist but can rather attach to the crystal as soon as the species desolvates. Adhesive growth occurs only above the roughening transition, also called the faceting transition, which corresponds to either a critical temperature or a critical supersaturation. Above the roughening transition, crystal surfaces have an intrinsic curvature and are atomically rough. Below the roughening transition, surfaces consist of steps separated by atomically smooth terraces (Akutsu and Yamamoto 2015). The faceted nature of zircon oscillatory zoning requires crystal growth below any roughening transitions.

Samples

The focus of this study are geologically young zircon crystals from the Adamello batholith in the Northern Italian Alps (sample PB775 and AS11 from Schaltegger et al. 2019) These zircon grains have been studied before (Schaltegger et al. 2019) and exhibit archetypal oscillatory zonation (Fig. 1). These crystals display no observable signs of radiation damage, cooled quickly, and did not subsequently undergo re-heating. Their U-Pb age of ca. 35 Ma suggests low estimates of long-term alpha-dose decay damage.

In the Adamello zircons, there is an inverse correlation between BSE and CL intensity such that BSE-bright zones are CL-dark zones, which we interpret to indicate that the CL-dark/BSE-bright zones are enriched in trace elements relative to the adjacent CL-bright/BSE-dark zones. Because it is well-established that BSE intensity only corresponds to mean atomic number, with higher intensities corresponding to higher mean atomic numbers, the oscillatory zoning reflects variation in impurity concentrations (Fig. 1).

Methods

Scanning electron microscopy (SEM)

SEM-BSE, -SE, and -CL images were acquired on a Helios Nanolab G3 at Utrecht University. Beam conditions were adjusted for each sample to optimize image quality and are recorded in the information bar burnt into each image as shown in Supplement 1, but generally ranged from: 7–20 kV accelerating voltage; 1.6–6.4 nA beam current; and 4.2–7.6 mm working distance.

(Scanning) transmission electron microscopy ((S)TEM)

Lamellae were milled from selected zircons using a Thermo Fischer Scientific (TFS) Helios 3G NanoLab focused-ion beam scanning electron microscope (FIB-SEM) and subsequently investigated using a TFS Talos 200FX transmission electron microscope (TEM) operated in scanning mode (STEM).

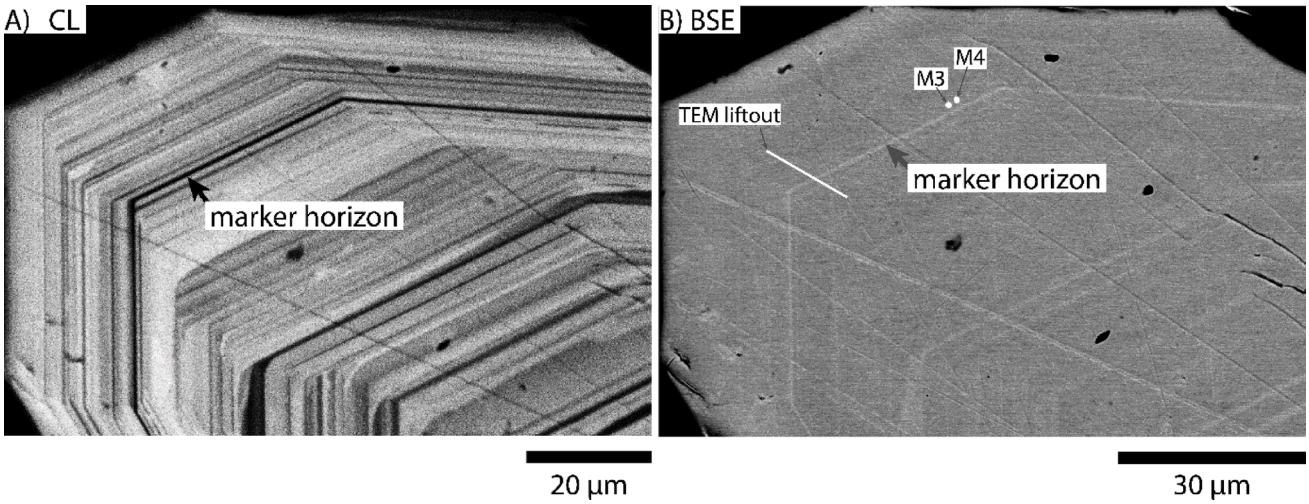

Fig. 1 Adamello zircon (PB775 15) shows distinct, archetypal euhedral oscillatory growth zones visible in both cathodoluminescent (CL) and backscattered electron (BSE) imaging. **A** In this zircon, high-impurity growth zones are CL-dark. **B** CL-dark, high-impurity growth zones are BSE-bright. Not all zones seen in CL are evident in the BSE image because of different dependencies of CL and BSE on impurity incorporation, the former being a complex interplay between bonding environment, defects, and lattice distortion and the latter being primarily dependent on mean atomic number. Annotations show the approximate locations of the TEM lift-out shown in Fig. 2, and the atom probe tips shown in Fig. 3. The marker horizon is the band intersected by the TEM and APT data

Monte Carlo beam convolution modelling

Beam convolution modelling was performed with DTSA-II. The sample geometry consisted of three adjacent growth zones: a 100 nm thick growth zone with 250 ppm Y, a middle 50 nm growth zone with 500 ppm Y, and a 125 nm growth zone with 250 ppm Y. The zones dipped 45° to the east from horizontal. The simulated 15 kV electron beam coincided with the center of the exposed 50 nm thick, 500 ppm Y central zone. 1000 electron trajectories were simulated.

Atom probe tomography (APT)

The easily identifiable marker horizon in PB775_15 intersected by (S)TEM foils was chosen as the target for APT specimens. The specimens were prepared using a Tescan Lyra3 Ga^+ FIB at Curtin University. The specimen location was carefully determined using electron-beam deposited Pt fiducials (Rickard et al. 2020). Specimens began in the low-impurity zone immediately adjacent to it and intersected the target high-impurity zone at an angle. The analysis was performed on the Geoscience Atom Probe, a Cameca LEAP 4000X HR at Curtin University (Reddy et al. 2020). The instrument was operated in laser-assisted mode with an ultraviolet (λ=355 nm) laser, pulsed at a repetition rate of 200 kHz with a pulse energy of 300 pJ. The specimens were maintained at a base temperature of 60 K and an automated detection rate of 0.01 ions/pulse was set for acquisition. The data was reconstructed with Cameca's AP Suite 6.3 software using a voltage evolution algorithm with a detector efficiency of 0.36, an image compression factor of 1.65, a k-factor of 3.3, an atomic volume of 0.01076 nm^3 per atom, and an empirically determined electric field of 32 V/nm (Fougerouse et al. 2022).

Results

Oscillatory zoning at the nanoscale

High-impurity growth zones appear homogeneous in SEM but reveal finer compositional layers under TEM (Fig. 2A). These layers are typically tens of nanometers in width (Supplemental Table 1) and include a bright inner zone (Fig. 2B, Supplement 2). The boundaries between the subzones are fuzzy in the (S)TEM images. In contrast, low-impurity growth zones are consistently homogeneous when imaged with TEM. Boundaries between low-impurity, CL-bright/BSE-dark zones and the composite CL-dark/BSE-bright high-impurity regions are sharp. No line or plane defects were observed in the TEM images, and the absence of radiation damage was confirmed.

Atom probe tomography (APT) of a series of tips oriented to intersect the CL-dark/BSE-bright marker horizon (Fig. 1) and the adjacent CL-bright/BSE-dark low-impurity zone, reveals that the low-impurity regions are homogeneous and defect-free at the atomic scale and that the interface between a low-impurity zone and a high-impurity zone is atomically sharp (Fig. 3), confirming observations made with the TEM (Fig. 2). Yttrium and uranium are the only elements that correlate with the zoning, and uranium is subtler than yttrium; other elements may also be zoned

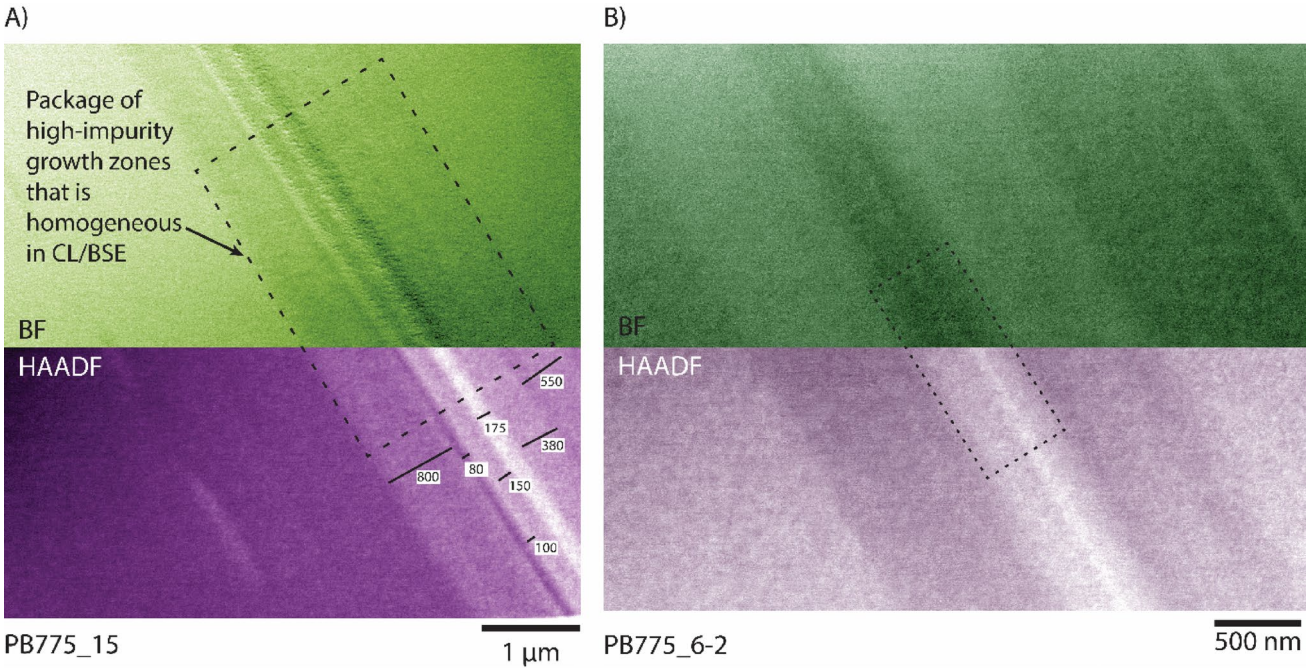

Fig. 2 These TEM samples are from two different zircon crystals from the same rock: PB775 15 and PB775 6−2. The dashed boxes outline sets of growth zones that appear to be homogeneous when imaged with a scanning electron microscope. **A** The seemingly homogeneous high-impurity CL-dark/BSE-bright marker horizon shown in Fig. 1 consists of a sequence of nanoscale growth zones when imaged with a transmission electron microscope. The upper falsely colored green image shows the growth zone as imaged with a bright field (BF) detector, while the lower falsely colored purple image shows that same growth zone as imaged with a high angle annular dark field (HAADF) detector. BF imaging produces phase contrast images and are sensitive to crystal structure and light elements, which are only weakly visible in HAADF. HAADF images are sensitive to atomic number (Z), with intensity increasing with Z2. Subzone widths in nm are marked on the HAADF image. **B** The simplest of CL-dark/BSE-bright zones are triplets consisting of two medium-impurity subzones and a central high-impurity subzone

but are unresolvable due to the relatively low mass resolving power of APT as a technique. Because of this, we do not attempt to quantify substitution mechanisms. Of 11 tips prepared, 6 yielded successful data (see Supplement). The APT data show essentially homogeneous distributions of trace elements within individual zones, which is consistent with TEM observations.

Just as the seemingly homogeneous CL-dark/BSE-bright high-impurity regions comprise smaller (~50–800 nm) growth zones when imaged with TEM, so are the zones imaged with TEM found to be made up of even smaller (~20–80 nm) zones when imaged with APT. These smallest zones are subtle, range in thickness from ~10–100 nm, and have fuzzy boundaries between them (Fig. 3).

Beam convolution modelling

Beam convolution is a well-understood phenomenon, but despite this the recognition that it may be obscuring the true nature of oscillatory growth zones has not been widely considered in models of zircon oscillatory growth (Melnik and Bindeman 2018; and references therein), although Fowler (2002) reported zones as thin as 195 nm imaged with SEM-BSE. Electron beam convolution limits the resolution that can be achieved with an SEM-CL - essentially, features that are smaller than the part of the interaction volume where the signals are being generated cannot be resolved. The nm-scale growth zones appear to be a single, homogeneous high-impurity growth zone when imaged with electron microscopy because they are planar features that are very small, dipping, and are closely spaced relative to the size of the beam interaction volume.

The interaction volume is the 3D region within a material where incoming electrons penetrate and interact with the material; the size and shape of the interaction volume depends on beam energy and the mean atomic number of the mineral. Each electron penetrates to a different depth within the solid, and as electrons penetrate into zircon, they generate, among other things: cathodoluminescence, characteristic X-rays, and backscattered electrons. The different signals are generated at different depths within the interaction volume (Fig. 4). BSE is generated at shallower penetration depths and horizontal distances than characteristic X-rays, which are generated at intermediate penetration depths and horizontal distances. Cathodoluminescence is generated at the farthest extents of the interaction volume

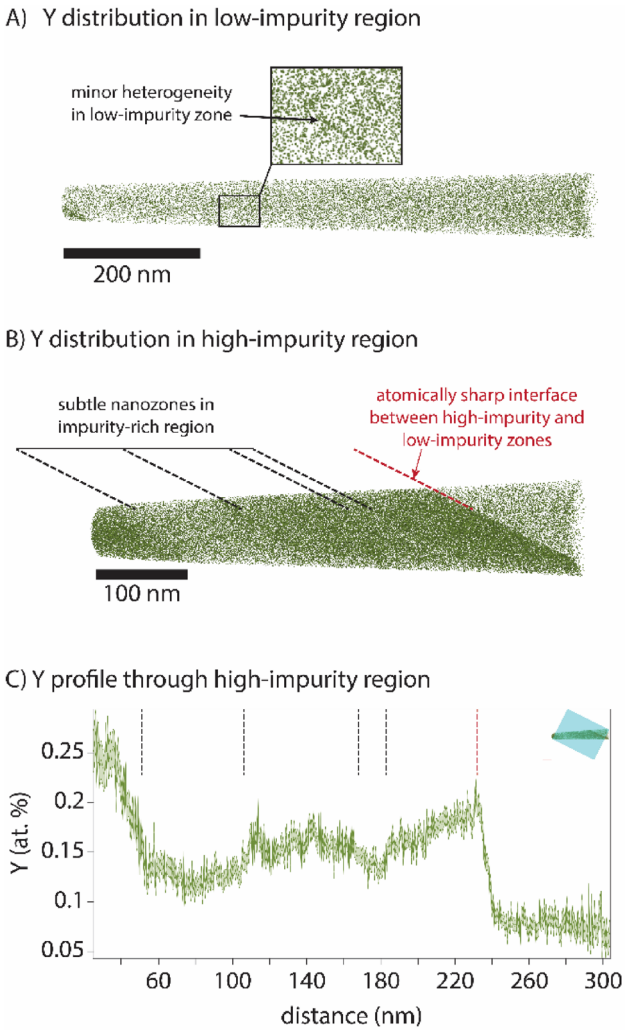

Fig. 3 **A** Atom probe tomography tip (M3) showing a low-impurity CL-bright/BSE-dark growth zone immediately adjacent to the high-impurity marker horizon. Low-impurity growth zones are remarkably defect free, showing only minor heterogeneities at the nanoscale. **B** Atom probe tomography tip (M4) showing part of the high-impurity growth zone. Boundaries between low-impurity and high-impurity growth zones are atomically sharp and lack dislocations. High impurity growth zones consist of smaller growth zones with more subtle, gradational boundaries between them. **C** A cross-sectional profile parallel to the length of the tip emphasizing the sharp nature of the interface between the high-impurity and low-impurity region and the more gradual changes in Y concentration that define subzones within the high-impurity region

due to the low activation energy required for phonon generation. Thus, for a given set of operating conditions, the signals have different spatial resolutions, which are, in order of highest to lowest spatial resolution: BSE, X-ray, CL.

Discussion

Fundamental limits on analytical resolution across techniques

The Monte Carlo electron simulations show that SEM-CL is lower resolution than SEM-BSE imaging. SEM imaging can only resolve features that are larger than the interaction volume over which the signal in question is being generated – thus, growth zones that are heterogeneous at scales smaller than electron beam interaction volumes appear to be homogeneous ('beam convolution'). (S)TEM does not suffer from beam convolution artefacts in the same way. (S)TEM samples are thinned to <150 nm thickness so that they are transparent to electrons; this essentially confines the interaction volume to the cross-section. Electrons pass through the sample with minimum lateral spread, minimizing interaction volumes so that it approximately matches the beam diameter. This is the reason that the (S)TEM images resolve zones that cannot be imaged with the SEM. However, (S)TEM imaging is limited by Z-contrast sensitivity and still averages signal from the <150 nm thickness of the sample, which obscures ultra-fine chemical variation. Nanoscale zones seen in the APT data, which is a time-of-flight mass spectrometry-based technique, are resolved by analyzing atoms layer-by-layer; APT has sub-nanometer resolution but cannot resolve features on the order of a unit cell.

Conceptual models of trace element incorporation during crystal growth

In crystals that grow slowly near thermodynamic equilibrium, trace element concentration depends on temperature, pressure, and bulk magma composition, and is independent of crystal surface reaction pathways. While the possibility of external changes in temperature, pressure, and melt composition cannot be completely excluded for some of the oscillatory zonations observed here, adopting such a hypothesis to explain the observed atom scale zoning would seem to require unrealistically large, sudden, and/or frequent changes, as previously noted by others for submicron scale effects (Hofmann et al. 2009; Yang et al. 2016).

When crystal growth is sufficiently fast to be in a non-equilibrium regime, trace element concentrations can be greater than or less than the equilibrium value, depending on diffusion and partitioning behavior. For example, when the rate of diffusion of yttrium (Y) in the melt is slow relative to the rate of zircon growth, a depletion halo of Y will form in the melt because this impurity partitions preferentially into zircon (partition coefficient generally >100; Claiborne et al. 2017), leading to sub-equilibrium Y concentrations.

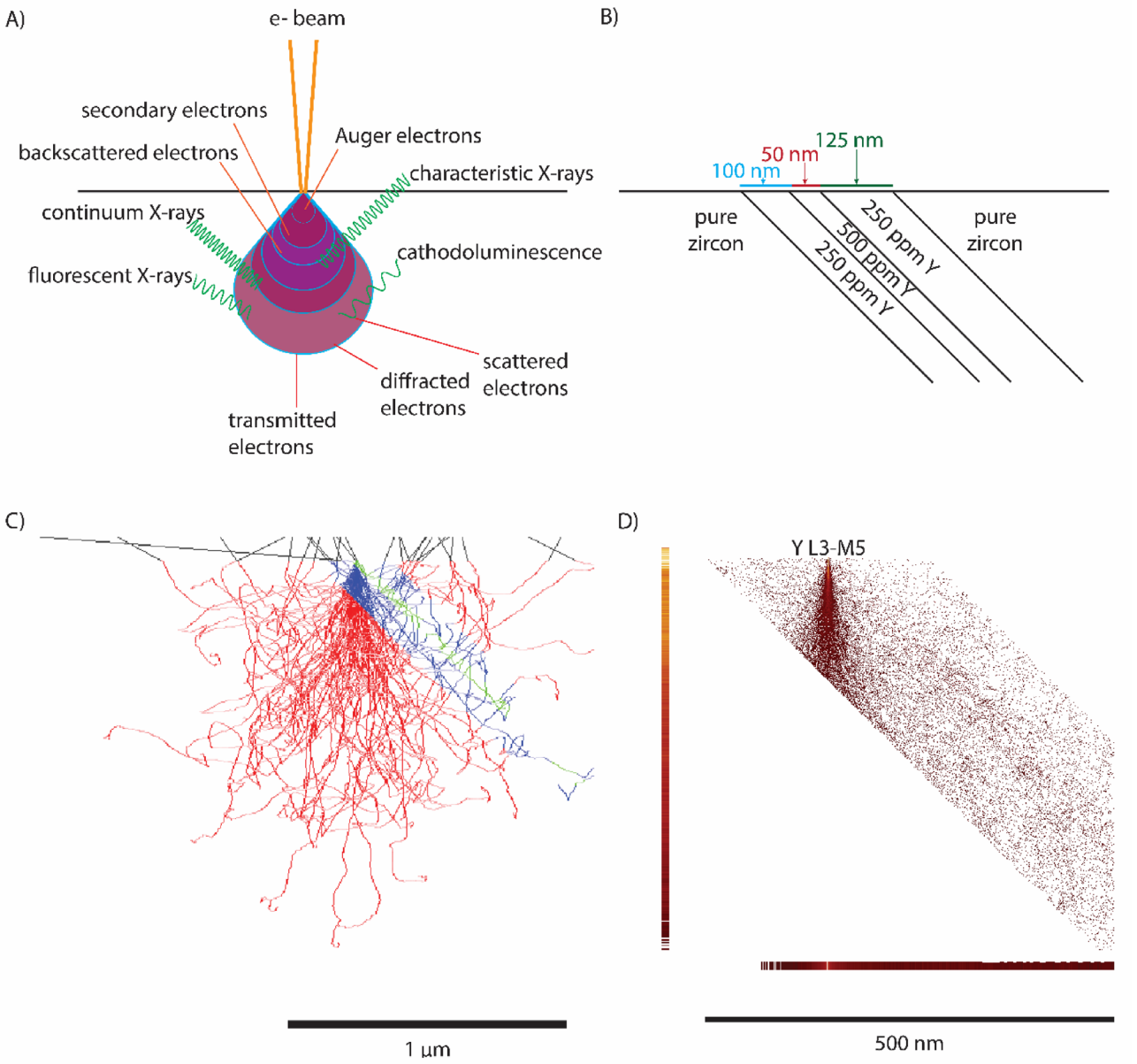

Fig. 4 DTSA-II kinetic Monte Carlo simulation of zoned zircon electron beam interaction volumes. **A** This not-to-scale schematic illustrates how different signals are generated over different portions of the interaction volume, with those requiring the highest activation energies occurring over smaller parts of the interaction volume and lower energy signals occurring over larger parts. **B** The model geometry used for the Monte Carlo simulation consists of pure zircon on either side of a triplet of growth zones. From left to right, the zones are 100 nm thick with 250 ppm Y, 50 nm thick with 500 ppm Y, and 125 nm thick with 250 ppm Y. Scale exaggerated for illustration. **C** The model electron beam was 1 nm in diameter, had an energy of 15 keV, and was directly incident on the 500 ppm Y growth zone. The image shows 1000 simulated electron trajectories. Red, blue, and green colors respectively indicate the location of pure zircon, the 250 ppm Y growth zones, and the 500 ppm growth zone. **D** A quantitative electron microprobe analysis averages the concentration over the interaction volume. The distribution of Y characteristic X-ray across the interaction volume is larger than the growth zones, so it is not possible to resolve the true spatial heterogeneity of the nm-scale impurity-rich zones. Backscattered electrons (BSE) are generated over a smaller portion of the interaction volume, so BSE images have slightly higher resolution than an X-ray map. Cathodoluminescence is generated over a larger portion of the interaction volume, so cathodoluminescent images have slightly lower resolution than BSE images or characteristic X-ray maps

At the same time, gradients in melt composition can arise from crystallization of other nearby phases. Since many other phases preferentially reject Y, it is conceivable that a nearby zircon might inherit Y in excess of the equilibrium value. These concepts were incorporated into a continuum model for diffusion-controlled zircon growth where various minor and trace elements (Hf, Y, U, Th, P, Dy) are passively incorporated into the crystal (Hoskin 2000; Melnik and

Bindeman 2018). This type of model can generate micron-scale oscillatory zonations but requires user-specified forcings such as oscillations in temperature or dissolved water content in the melt.

A key assumption of most diffusion-controlled crystal growth models, which may warrant reconsideration in light of our finding that high-impurity zones are made of smaller zones to the nanoscale, is local equilibrium at the crystal-melt interface. There is ample evidence from crystal growth experiments that partitioning at the crystal-fluid interface depends on growth rate, suggesting that impurities are entrapped before they establish local equilibrium, e.g., Sr in calcite (Tang et al. 2008), Ti in quartz (Huang and Audetat 2012), and Ge and Al in quartz (Phelps et al. 2019). It is therefore possible for fluctuations in growth rate to produce oscillatory zonations, but such a scenario would still seem to require an external forcing that would cause fluctuations in growth rate. An additional consideration, however, is that trace elements themselves can affect growth rate, leading to feedbacks that have been considered in the materials science and crystal growth literature but have not been adequately explored for natural silicate minerals.

Our TEM/APT data favors an impurity poisoning interpretation for oscillations in impurity incorporation during growth because it shows that CL-dark/BSE-bright growth zones are made of finer zones that are approximate interplanar d-spacings in thickness, which is an expected feature of growth zones formed by impurity-step dynamics. However, further investigation is necessary to work out which subzones correspond to which kinds of steps, the interplay between element diffusion and step dynamics, and how fluctuations of pressure, temperature and composition influence local supersaturation, including consideration of the influence on step curvature of impurities with different adsorption times. Natural crystals form from fluids that contain multiple types of impurities, and the interplay between different types of adsorbates is poorly constrained (which is why we have made no attempt to do so in this contribution).

Impurity poisoning in the dead zone

General framework

Impurity poisoning has been previously suggested as the kinetic mechanism whereby oscillatory zoning forms in zircon (Hanchar et al. 2001) and, notably, the general case has recently been modeled by Torii and Miura (2024). It is worthwhile to take the time to thoroughly review the current state of knowledge because although it is well-established, it is not generally known to the wider geology audience, nor is it widely incorporated into petrogenetic models and interpretations.

The terrace-ledge-kink (TLK) model categorizes mineral surface growth sites by their relative reactivity, which is determined by the number of satisfied versus unsatisfied bonds (Fig. 5A). The energy necessary to liberate an atom from a crystal surface depends on the number of other atoms to which it is bonded. The attraction of an attachment site is governed by the coordination number of the site, which can be conceptualized as being inverse to the number of unsatisfied bonds at the site. Atoms within the bulk of a crystal are surrounded by other atoms and so are difficult to dislodge from the lattice; these sites are not reactive at all. Terrace vacancies are bound to the lattice in all directions but one and have many neighbors and the few unsatisfied bonds. In mineral-fluid systems, terrace terminations are solvated or bound to species in solution. Atoms at step ledges have fewer neighbors and more unsatisfied bonds, making them more reactive than terrace vacancies. Kink sites, which are like the corners of ledges, have the fewest neighbors and the most unsatisfied bonds, making them the most reactive of attachment sites. Kink sites and ledges are where most atoms attach to the crystal.

Faceted crystals grow by the lateral advance of a layer of atoms on top of an existing crystal. The raised ledges of these layers are where there are unsatisfied bonds, and so the raised ledge, which is called a step, flows across the crystal surface as elements attach to the step ledge.

The smallest of steps is a microstep, also called an elementary step, which is equal in height to the interplanar d-spacing of the crystal face is under consideration. Steps nucleate at outcropping crystal defects and propagate outward. Where there are multiple step nucleation sites (step sources), steps ripple out and converge with one another. Microstep velocity is a function of supersaturation at the interface and the concentration of adsorbed impurities at step ledges.

Step bunching, where steps become closely-spaced, advanced as a train, and ultimately become close enough to merge into a macrostep, can result from a number of effects (Sunagawa 2007): supersaturation fluctuations at the growth interface and surface diffusion with respect to the upper and lower step terraces (the Ehrlich-Schwoebel effect; cf. Sato and Uwaha 2001), the presence of foreign particles adhered to the growth surface (inclusions), and adsorbed impurities. Step bunching produces macrosteps. Microsteps that overtake other steps due to differences in velocity pile on top of one another to create macrosteps, a second class of steps with heights that are integer multiples of the interplanar d-spacing. Macrostep dynamics differ from those of microsteps in the details of the step velocity dependence on supersaturation - generally though, they advance more slowly than microsteps. In some systems, macrosteps converge with other macrosteps to form supersteps, which

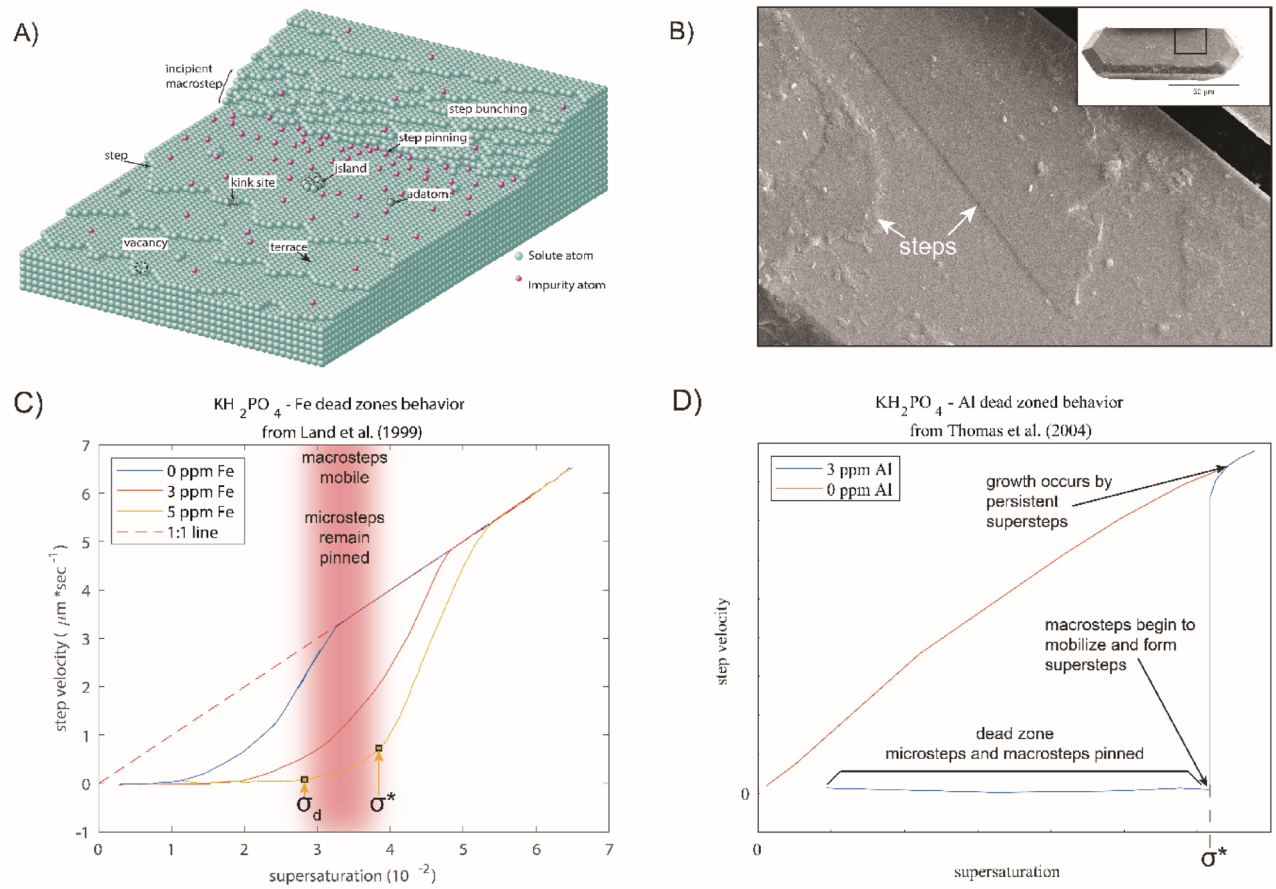

Fig. 5 **A** Conception of a crystal growth surface in the terrace-ledge-kink framework consists of terraces, ledges, kinks, adatoms, and vacancies. During faceted crystal growth, step ledges are the most abundant attachment site on the growth surface and the primary direction of atomic attachment is parallel to the surface rather than perpendicular to it. The vertical red arrow denotes the growth rate normal to the crystal surface, R, and the horizontal arrow denotes the velocity of the flowing step, v. **B** Scanning electron microscope secondary electron images of a zircon from Adamello identifying what we interpret to be growth steps preserved on the surface of the crystal. **C** KDP crystals poisoned by iron recover from the dead zone by mobile macrosteps in the range $\sigma d - \sigma *$. Modified from Land et al. (1999). **D** KDP crystals poisoned by aluminum recover from the dead zone by the formation and rapid propagation of supersteps. Modified from Thomas et al. (2004a, b)

are 50-1500 microsteps tall and unique in their dynamics (Thomas et al. 2004a, b). Steps are preserved on the surfaces of faceted crystals and can be seen with the naked eye, as is the case for quartz and pyrite striations, or with microscopic imaging, as is the case for zircon (Fig. 5B).

Dead zone dynamics

Impurity poisoning occurs where adsorbed impurities arrest step movement across a crystal facet. It can manifest as the dead zone—a range of supersaturations wherein crystal growth does not occur, even in the presence of seed crystals. Step dynamics in the dead zone, and recovery from it, depend on the duration of attachment of adsorbed impurities.

Step pinning occurs where impurities adsorbed to terraces impede step growth because the impurities create localized energy barriers that the advancing steps must overcome (Ranganathan and Weeks 2013). Impurities at terraces may be held by a combination of Van der Waals forces, electrostatic interactions, solvent-mediated interactions, and surface defects. As an advancing step encounters an adsorbed impurity, it either incorporates the impurity or curves around it. If the step curves around the impurity, the increase in curvature raises the chemical potential of the step which makes it more difficult for new atoms to attach. This is described mathematically by the Gibbs-Thompson equation:

$$\mu_{step} = g\mathrm{W}k \tag{1}$$

where μ_{step} is the chemical potential of the curved step, γ is the surface energy at the step ledge, Ω is the atomic volume, and κ is the step curvature. Tighter curves are caused by higher density of adsorbed impurities; the tighter the curve

the more significant the increase in chemical potential (De Yoreo and Vekilov 2003). The relationship between chemical potential and supersaturation is given by:

$$\sigma = \frac{\Delta \mu_{effective}}{kT} \quad (2)$$

where k is Boltzmann's constant and T is the absolute temperature. Increased step chemical potential reduces the effective supersaturation ($\Delta\mu_{effective} = \mu_{environment} - \mu_{step}$, where $\mu_{environment}$ is the chemical potential of the component in the ambient environment/fluid). At low impurity concentrations, impurities can be incorporated into the crystal lattice as they diffuse across the facet and encounter kink sites.

Step dynamics for idealized Kossel crystals have been investigated using atomistic kinetic Monte Carlo (kMC) simulations, revealing behaviors that are overlooked by mean field approaches or in analytical expressions (Lutsko et al. 2016; Sleutel et al. 2017; Lutsko and Maes 2023). For example, solute attachment to the vertical face of a pinned macrostep can provide a mechanism for the step to begin to advance laterally again and so recover from the dead zone (Lutsko et al. 2016; Sleutel et al. 2017). The kMC simulations show the advance of macrosteps can produce atomic scale chemical banding at a given supersaturation (i.e., without external forcing) via step dynamics alone (Sleutel et al. 2017).

Experimental poisoning of KDP crystals: an accessible analogue for zircon?

To our knowledge at this time, dead zones have not been systematically measured for geologically relevant systems, but the phenomenon has been studied extensively by chemists in low-temperature growth of crystalline solids from aqueous solutions. One of the most well-studied dead zones is that of potassium dihydrogen phosphate (KDP; KH_2PO_4).

Experiments on the poisoning of KDP growth in aqueous solutions by trivalent metals indicate that impurities with longer adsorption times exit the dead zone by macrosteps and that impurities with shorter adsorption times exit the dead zone by supersteps. These studies focus on KDP-supersaturated aqueous solutions with trace amounts of impurities. Chemical systems with significant concentrations of more components, like silicate magmas, will almost certainly exhibit more complex behavior. Although impurity poisoning of zircon precipitating from a felsic silicate melt will differ from experimentally investigated poisoning of crystals precipitating from aqueous systems under well-controlled laboratory conditions, it is reasonable to assume that, to a first order, all faceted crystals grow via the essentially same mechanisms and so analogous systems may be instructive even if the results aren't exactly applicable to zircon.

Using in situ atomic force microscopy to examine KDP growth in the presence of Fe^{3+}, Land et al. (1999) found that KDP recovered from the iron-induced dead zone through gradual acceleration of macrosteps that were about 10–12 microsteps tall. The range of supersaturations spanned by a dead zone is proportional to the square root of impurity concentration: $\sigma_d \propto C_i$ (Fig. 5C; De Yoreo and Vekilov 2003). The sequence of step events, in overview, is as follows (Fig. 5C):

1. When supersaturation is less than some critical value ($\sigma < \sigma_d$) growth is negligible on experimental time scales. Microsteps and macrosteps are present and pinned, as indicated by the development of curvature along step ledges. This is the dead zone.

Although growth is taken to be immeasurably slow in dead zone experiments, over geologic time scales it may be significant. If that is true, then this would represent near-equilibrium growth and formation of zircon CL-dark/BSE-bright low-impurity zones.

Steps would incorporate impurities according to equilibrium partitioning, rejecting excess impurities from the bulk of the crystal. Rejected impurities adsorb to step ledges; impurity concentration at the crystal-fluid interface is a function of the relative rates of impurity attachment and detachment, diffusivity in the fluid, and crystal growth rate. Impurity enrichment at step ledges could be a natural consequence of near-equilibrium growth.

2. As supersaturation increases beyond the critical value ($\sigma_d < \sigma < \sigma^*$) - maybe due to diffusion across the boundary layer, changes in melt polymerization, small temperature or pressure fluctuations, etc. - microsteps remain practically immobile but macrosteps become mobile. Growth begins again, albeit not at the rate predicted for a pure system. As macrosteps advance, they incorporate pinned elementary steps and presumably, the impurities that pinned them, into the bulk of the crystal at their bottom edge. The consumed microstep becomes the leading edge of the macrostep. The surface behind a macrostep consists of elementary steps separated from the top of the macrostep as impurities attached to the top step pin it in some places. Macrostep height is roughly constant because microsteps become pinned and are shed from the top of the macrostep at roughly the same rate that pinned microsteps are incorporated into the bottom of the macrostep and become the leading edge.
3. At supersaturations near σ^*, macrostep velocity increases with supersaturation and macrostep ledges

become progressively straighter. Microsteps begin to straighten and become mobile, but their velocity is much slower than the velocity of coexisting macrosteps.
4. At sufficiently high supersaturation ($\sigma > \sigma^*$), microsteps and macrosteps are both mobile and have similar step velocities. Step velocities increase rapidly and approach those of the pure system as supersaturation increases further.

In a set of similar experiments that examined KDP poisoning by Al^{3+}, which was found to have a shorter adsorption time, Thomas et al. (2004a, b) recorded the supersteps formation during recovery from the dead zone at precisely σ^* (Fig. 5D):

1. Below σ^* microsteps and macrosteps are present and immobile. This is the dead zone, which is large because there is no range of supersaturations over which macrosteps are mobile as microsteps remain pinned.
2. At σ^* macrosteps begin to move as elementary steps become pinned. Supersteps emerge at precisely this point, consisting of 100's −1000's of tightly spaced microsteps that advance as a single step. Observed supersteps were up to 500 nm tall, which is equivalent to about 1350 microsteps for the KDP {100} face. Superstep movement at σ^* is erratic and superstep height is variable. Superstep velocity rapidly increases with a very small increase in supersaturation (near-vertical line on Fig. 5D).
3. Above the dead zone ($\sigma > \sigma^*$), superstep velocities are approximately equal to those of microsteps and macrostep in the undoped system. Supersteps leave behind atomically smooth terraces as they flow across the surface ("surface cleansing", Ranganathan and Weeks 2013); they do not "shed" their uppermost microstep as the macrosteps from Land et al. (1999) did.

The details of how impurities influence step dynamics during crystal growth are determined by the relative rates of crystal growth, element diffusion through the melt, and the adsorption and desorption rates of impurities at the crystal surface. The KDP experiments summarized in this section are specific to Fe^{+3} or Al^{+3} interacting with KDP and are variations on the theme of impurity poisoning. Although impurity poisoning has not yet been experimentally studied in zircon, or even directly observed during magmatic growth, insights from model systems such as KDP are relevant because faceted crystal growth almost certainly occurs via the same essential processes universally. The fact that oscillatory growth zones occur in a variety of geologic systems and minerals hints at the universal nature of impurity effects on faceted crystal growth; the terrace-ledge-kink framework and step dynamics responsible for impurity poisoning are fundamental to the growth of all faceted crystals. Therefore, even though impurity poisoning has not yet been experimentally studied in zircon, we infer that the principles demonstrated in KDP experiments are transferable to zircon and other minerals, providing a general framework for understanding oscillatory zoning in geologic materials.

Impurity poisoning and zircon zoning

Our finding that CL-dark/BSE-bright zones are composites of finer zones with atomically sharp boundaries down to the nm scale while CL-bright/BSE-dark zones are homogeneous across all resolutions suggests that fine-scale oscillatory growth zones are a consequence of faceted, near-equilibrium growth in impurity-bearing systems. The atomically sharp interfaces between zircon growth zones shown in our APT data, and in the APT data of Foley et al. (2024) cannot be explained by an adhesive growth mechanism because adhesive growth does not form flat surfaces. Growth models that fail to incorporate faceted growth mechanisms in favor of adhesive growth cannot recreate the processes whereby trace element oscillatory growth zones form because they ignore the kinetic complexity of step interactions and processes such as surface diffusion. We note that this does not necessarily extend to minerals such as plagioclase, where major element growth zoning is common, and restrict our interpretations to impurity-mineral interactions rather than solid solutions. Our findings suggest that oscillatory zoned magmatic zircon growth does not always, or even usually, occur by an adhesive growth mechanism but rather either a 2D nucleation and growth mechanism or a spiral growth mechanism (García-Ruiz and Otálora 2015; Sunagawa 1981). Impurity poisoning still requires changes in local supersaturation, which could be driven by fluctuations in pressure, temperature, or diffusion. However, the isothermal, isobaric, constant composition oscillatory zoned calcite from the Barker and Cox (2011) experiments suggests that in some situations oscillations may form in the absence of external forcing.

Impurity poisoning has not been experimentally investigated as a mechanism for zircon oscillatory growth in felsic magmatic systems; it would be very challenging to successfully emulate the time scales and supersaturation conditions of near-equilibrium zircon growth. However, the fundamental mechanisms of crystal growth processes are universal, so it stands to reason that many, if not all, trace element oscillatory zoned crystals form via the same mechanism. Processes of growth steps interacting with adsorbed impurities must occur wherever a faceted crystal grows from an impure solution.

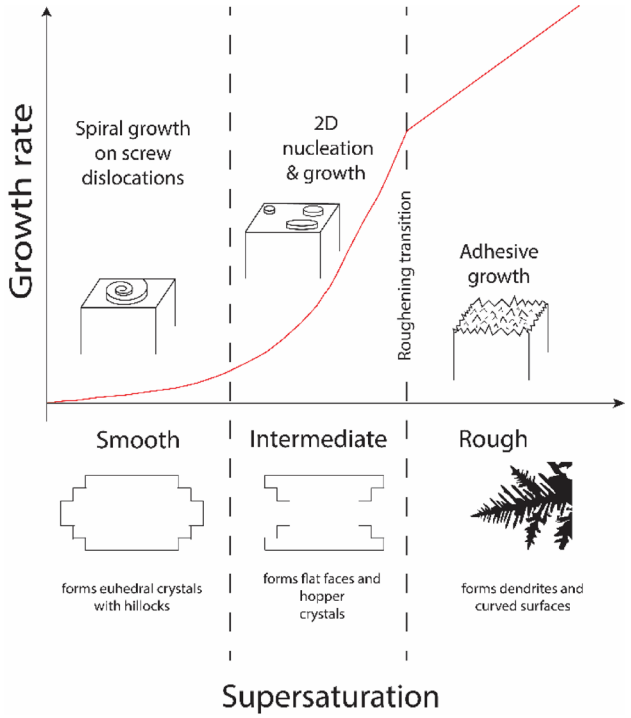

Fig. 6 Generally speaking, there are three unique growth mechanisms, each of which operates over a unique range of supersaturations and has a unique growth rate dependence on supersaturation. Faceted growth occurs below the roughening transition by either the spiral growth mechanism or 2D nucleation and growth. In spiral growth, layers nucleate on outcropping screw dislocations in the center of faces and flow outwards towards the edges of the face. In 2D nucleation and growth, layers nucleate at defects near the edges of crystal faces, or on the edges themselves, and flow towards the centers. Above the roughening transition, growth occurs by the adhesive mechanism. Roughening transitions can be kinetic or thermal. Thermal roughening occurs above a critical temperature and kinetic roughening occurs above a critical supersaturation. The growth surface is curved and consists primarily of highly reactive kink sites. In this regime, surface diffusion is negligible. Ti zoning of magmatic quartz phenocrysts with curved faces is a common example of growth zoning formed by an adhesive growth mechanism (Peppard et al. 2001)

Comparison to trace element oscillations in hydrothermal minerals

Faceted trace element oscillatory growth zones are ubiquitous in geologic systems, occurring in magmatic, metamorphic (George et al. 2024), sedimentary (Bryksina et al. 2006), and hydrothermal systems (Acosta et al. 2022). It is possible that the underlying process responsible for impurity oscillations is the same across all of these systems because in each case the euhedral textures record faceted growth, whereby growth occurs via steps (not an adhesive growth mechanism) and the growth mechanism ise either 2D nucleation and growth or spiral growth. This further necessitates that the supersaturation and temperature be such that the crystal surface is below its kinetic or thermal roughening transition (Fig. 6). The comparison with low temperature minerals precipitated from hydrothermal fluids is especially intriguing because element diffusivities are much faster in aqueous fluids than in silicate melts (Aniceto et al. 2024) and the hydrothermal fluids are commonly flowing. We posit that impurity-induced growth inhibition is a universal process, and the fact that similar oscillatory faceted growth zoning is observed in hydrothermal minerals as in zircons precipitated from felsic magmatic systems underscores that faceted crystal growth occurs via universal mechanisms regardless of the structure of the fluid that a given crystal is precipitating from, even in systems where diffusion across a boundary layer in the fluid is unlikely to be significant.

In a study of hydrothermal quartz in the Butte porphyry copper deposit, Acosta et al. (2022) argued that oscillatory Ti growth zones cannot be due to equilibrium growth at any realistic pressure or temperature, and that high impurity growth zones must result from a kinetic effect. Oxygen isotope ratios do not vary across hydrothermal quartz oscillatory growth zones from the Haquira East porphyry Cu deposit (Cernuschi et al. 2018), indicating that temperatures were relatively constant during their formation. Because porphyry Cu deposits form through cycles of hydrofracturing events, rapid pressure changes occur that can cause rapid changes in quartz growth rate, and so one reasonable interpretation is that each high impurity zone records a pressure drop. It is important to note that the high-impurity layers in hydrothermal quartz require surface enrichment because the concentrations are higher than what can be produced by diffusive exchange across an aqueous boundary layer alone.

Calcite stands out as a mineral for which faceted growth mechanisms have been thoroughly investigated experimentally. Mn is preferentially incorporated into slower steps, causing variation in crystal morphology and growth rates (Astilleros et al. 2002). In one set of experiments by Barker and Cox (2011) oscillatory REE zoning formed during isothermal and isobaric crystal growth from solution indicating that minerals precipitating from aqueous solutions can form oscillatory growth zoning in the absence of significant fluctuations in composition, pressure, and temperature.

Implications for geochronology and further work

It is beyond the scope of this contribution to fully explore the implications of impurity poisoning on zircon U-Pb geochronology systematics. The APT data show that U is enriched at the nanoscale along with Y, suggesting that U incorporation may be influenced by impurity poisoning events. However, even the smallest resolution techniques for in-situ spot-analysis for U-Pb geochronology (e.g., SIMS) average U and Pb ratios over volumes that are much larger than the finest-scale zoning so that the analyses are mixtures of the

high- and low-impurity nanoscale zones. It is not clear what the timescales of impurity poisoning events are, but studies showing that U-Pb dates are continuous across oscillatory zoned zircon from core-to-rim (e.g., Mattinson et al. 1996; Aleinikoff et al. 2001) suggest that they may occur on timescales that are essentially instantaneous with respect to the precision of in situ U-Pb geochronology techniques. In other words, oscillatory zoning doesn't necessarily equate to intra-grain U-Pb date heterogeneity. However, U-rich growth zones are more likely to experience more alpha-dose radiation damage and subsequent Pb mobilization.

Within the framework of impurity poisoning, recovery from the dead zone traps impurities enriched at the crystal-fluid interface so the boundary layer composition is likely to differ significantly from that of the bulk melt. Incorporating this process into models of trace element uptake during crystal growth is an important next step towards understanding how to use disequilibrium trace element enrichments to unravel magmatic evolution. Quantitatively untangling kinetic impurity poisoning effects from compositional fluid changes is likely to be a complex problem. There are many additional open questions about how impurity poisoning occurs, especially in magmatic systems where multiple trace elements are interacting with steps. The (S)TEM images show a lot of variability in subzone sequences and thicknesses, and it remains to be seen how that heterogeneity fits into the framework of this hypothesis. Step dynamics are complex and not independent of boundary layer diffusion and system-scale fluctuations in temperature, pressure, and composition.

Further studies focused on the characterization of zircon oscillatory growth zoning should incorporate comprehensive studies of zircon step patterns using a step decoration method, more targeted APT profiles (maybe by creating tips directly from the TEM lamellae) and on characterizing more zircons from different geologic environments to constrain whether or not the crystals studied in this contribution are typical of oscillatory zoned minerals in general. Other unknowns include the time scales of zircon poisoning and recovery events, multi-element interactions, and whether or not other oscillatory zoned minerals display the same self-affine fractal nature as zircon.

Conclusions

We find that high-impurity CL-dark/BSE-bright zircon oscillatory growth zones are self-affine to the nanoscale: zones that are homogeneous in SEM images are made up of smaller and smaller zones when imaged with TEM and APT. Low-impurity CL-bright/BSE-dark zones remain homogeneous across all analytical resolutions. Interfaces between high-impurity and low-impurity zones are planar and atomically sharp at the nanoscale, a feature which is masked in SEM images due to beam convolution and which precludes diffusion in a boundary layer as the primary mechanism whereby oscillatory growth zoning forms. Within the well-established framework of terrace-ledge-kink theory, the universal crystal growth phenomenon of impurity poisoning can explain the self-affine zoning down to d-spacing scales and the atomically sharp, planar interfaces between adjacent zones. Although there are no existing experimental studies focused on zircon impurity poisoning, we suggest that any faceted crystal growing at a low supersaturation in the presence of adsorbed impurities can undergo growth hysteresis in the dead zone as impurities interfere with step flow processes. Within this framework, high impurity zones reflect kinetic entrapment, rather than equilibrium thermodynamic partitioning.

This contribution bridges materials science, chemistry, and geoscience approaches to understanding how crystals incorporate impurities and demonstrates the need for multi-scale analytical approaches.

Supplementary Information The online version contains supplementary material available at https://doi.org/10.1007/s00410-025-02288-4.

Acknowledgements We thank Urs Schaltegger for providing the Adamello zircon samples. Nicholas Ritchie assisted with running the DTSA-II Monte Carlo simulations. We thank Markus Ohl for his assistance with TEM data collection via the EXCITE network. We thank the editor and two anonymous reviewers for their contributions improving this manuscript.

Author contributions Authors Acosta, Watkins, and Reed contributed to study conception and design. Material preparation and data collection was performed by authors Fougerouse, Saxey, Plümper, and Reddy. All authors contributed to data analysis. The manuscript was written by Acosta and all authors edited and commented on subsequent versions of the manuscript.

Funding This research was funded by two rounds of EXCITE network support: the TEM data acquisition was supported by project number EXCITE C2_2022_13 and the APT data acquisition was supported by project number E2-1-68.

Declarations

Conflict of interest The authors have no competing interests to declare that are relevant to the content of this article.

References

Acosta M, Reed M, Watkins J (2022) Quartz vein formation and deformation during porphyry Cu deposit formation: a microstructural and geochemical analysis of the Butte, Montana, ore deposit. Lithosphere 2022:3196601. https://doi.org/10.2113/2022/3196601

Akutsu N, Yamamoto T (2015) Rough–smooth transition of step and surface. In: Nishinaga T (ed) Handbook of crystal growth, 2nd edn. Elsevier, pp 265–313. https://doi.org/10.1016/B978-0-444-56369-9.00006-X

Aleinikoff JN, Wintsch RP, Fanning CM, Dorais MJ (2002) U–Pb geochronology of Zircon and polygenetic titanite from the Glastonbury Complex, Connecticut, USA: an integrated SEM, EMPA, TIMS, and SHRIMP study. Chem Geol 188(1–2):125–147

Allègre CJ, Provost A, Jaupart C (1981) Oscillatory zoning: a pathological case of crystal growth. Nature 294:223–228. https://doi.org/10.1038/294223a0

Aniceto JP, Zézere B, Silva CM (2024) Prediction of diffusion coefficients in aqueous systems by machine learning models. J Mol Liq 405:125009. https://doi.org/10.1016/j.molliq.2024.125009

Astilleros JM, Pina CM, Fernández-Díaz L, Putnis A (2002) Molecular-scale surface processes during the growth of calcite in the presence of manganese. Geochim Cosmochim Acta 66:3177–3189. https://doi.org/10.1016/S0016-7037(02)00892-X

Barker SL, Cox SF (2011) Oscillatory zoning and trace element incorporation in hydrothermal minerals: insights from calcite growth experiments. Geofluids 11:48–56. https://doi.org/10.1111/j.1468-8123.2010.00305.x

Bryksina NA, Halden NM, Mejia S (2006) Qualitative and quantitative characteristics of modeled and natural oscillatory zoning patterns in calcite. Math Geol 38:635–655

Burton WK, Cabrera N, Frank FC (1951) The growth of crystals and the equilibrium structure of their surfaces. Philos Trans R Soc Lond Math Phys Sci 243:299–358. https://doi.org/10.1098/rsta.1951.0006

Carley TL, Miller CF, Wooden JL, Bindeman IN, Barth AP (2011) Zircon from historic eruptions in iceland: reconstructing storage and evolution of silicic magmas. Mineral Petrol 102:135–161. https://doi.org/10.1007/s00710-011-0169-3

Cernuschi F, Dilles JH, Grocke SB, Valley JW, Kitajima K, Tepley FJ (2018) Rapid formation of porphyry copper deposits evidenced by diffusion of oxygen and titanium in quartz. Geology 46:611–614. https://doi.org/10.1130/G40262.1

Chernov AA (1961) The spiral growth of crystals. Sov Phys Usp 4:116

Chernov AA (1984) Growth mechanisms. In: Modern Crystallography III: Crystal Growth, pp 104–158. https://doi.org/10.1007/978-3-642-81835-6_3

Claiborne LL, Miller CF, Wooden JL (2010) Trace element composition of igneous zircon: a thermal and compositional record of the accumulation and evolution of a large silicic batholith, spirit mountain. Contrib Mineral Petrol 160:511–531. https://doi.org/10.1007/s00410-010-0491-5

Claiborne LL, Miller CF, Gualda GAR, Carley TL, Covey AK, Wooden JL, Fleming MA (2017) Zircon as magma monitor: robust, temperature-dependent partition coefficients from glass and Zircon surface and rim measurements from natural systems. In: Moser DE, Corfu F, Darling JR, Reddy SM, Tait K (eds) Microstructural geochronology: planetary records down to atom scale. Wiley, pp 1–33. https://doi.org/10.1002/9781119227250.ch1

Corfu F, Hanchar JM, Hoskin PWO, Kinny P (2003) Atlas of Zircon textures. Rev Mineral Geochem 53:469–500. https://doi.org/10.2113/0530469

De Yoreo JJ, Vekilov PG (2003) Principles of crystal nucleation and growth. Rev Mineral Geochem 54:57–93. https://doi.org/10.2113/0540057

Foley ML, Bloch EM, Gerstl SS, Putlitz B, Baumgartner LP (2024) Integrated textural and geochemical analysis of igneous Zircon by atom probe tomography. Contrib Mineral Petrol 179:19. https://doi.org/10.1007/s00410-024-02166-5

Fougerouse D, Saxey DW, Rickard WD, Reddy SM, Verberne R (2022) Standardizing Spatial reconstruction parameters for the atom probe analysis of common minerals. Microsc Microanal 28:1221–1230. https://doi.org/10.1017/S1431927621013714

Fowler A, Prokoph A, Stern R, Dupuis C (2002) Organization of oscillatory zoning in Zircon: analysis, scaling, geochemistry, and model of a Zircon from Kipawa, Quebec, Canada. Geochim Cosmochim Acta 66:311–328. https://doi.org/10.1016/S0016-7037(01)00774-8

García-Ruiz JM, Otálora F (2015) Crystal growth in geology: patterns on the rocks. In: Nishinaga T (ed) Handbook of crystal growth: bulk crystal growth, vol 2, 2nd edn. Elsevier, pp 1–43. https://doi.org/10.1016/B978-0-444-63303-3.00001-8

George FR, Viete DR, Avila J, Seward GG, Guice GL, Allen MB, Harrower MJ (2024) Garnet zoning patterns record multiple processes of chemical transfer during subduction. Earth Planet Sci Lett 631:118634. https://doi.org/10.1016/j.epsl.2024.118634

Halden NM, Hawthorne FC (1993) The fractal geometry of oscillatory zoning in crystals: application to Zircon. Am Mineral 78:1113–1116

Hanchar JM, Finch RJ, Hoskin PWO, Watson EB, Cherniak DJ, Mariano AN (2001) Rare Earth elements in synthetic zircon: part 1. Synthesis, and rare Earth element and phosphorus doping. Am Mineral 86:667–680

Hofmann AE, Valley JW, Watson EB, Cavosie AJ, Eiler JM (2009) Sub-micron scale distributions of trace elements in Zircon. Contrib Mineral Petrol 158:317–335. https://doi.org/10.1007/s00410-009-0385-6

Holten T, Jamtveit B, Meakin P, Cortini M, Blundy J, Austrheim H (1997) Statistical characteristics and origin of oscillatory zoning in crystals. Am Mineral 82:596–606

Hoskin PW (2000) Patterns of chaos: fractal statistics and the oscillatory chemistry of Zircon. Geochim Cosmochim Acta 64:1905–1923. https://doi.org/10.1016/S0016-7037(00)00330-6

Hoskin PW, Schaltegger U (2003) The composition of Zircon and igneous and metamorphic petrogenesis. Rev Mineral Geochem 53:27–62. https://doi.org/10.2113/0530027

Huang R, Audéétat A (2012) The titanium-in-quartz(TitaniQ) thermobarometer: A critical examination and re-calibration. Geochimica etCosmochimica Acta 84:75-89.

L'Heureux I (1993) Oscillatory zoning in crystal growth: a constitutional undercooling mechanism. Phys Rev E 48:4460–4469. https://doi.org/10.1103/PhysRevE.48.4460

L'Heureux I, Fowler AD (1996) Dynamical model of oscillatory zoning in plagioclase with nonlinear partition relation. Geophys Res Lett 23:17–20. https://doi.org/10.1029/95GL03327

L'Heureux I, Jamtveit B (2002) A model of oscillatory zoning in solid solutions grown from aqueous solutions: applications to the (Ba,Sr)SO4 system. Geochim Cosmochim Acta 66:417–429. https://doi.org/10.1016/S0016-7037(01)00792-X

L'Heureux I, Katsev S (2006) Oscillatory zoning in a (Ba,Sr)SO4 solid solution: macroscopic and cellular automata models. Chem Geol 225:230–243. https://doi.org/10.1016/j.chemgeo.2005.08.017

Land TA, Martin TL, Potapenko S, Palmore GT, De Yoreo JJ (1999) Recovery of surfaces from impurity poisoning during crystal growth. Nature 399:442–445. https://doi.org/10.1038/20886

Loewen MW, Bindeman IN (2016) Oxygen isotope thermometry reveals high magmatic temperatures and short residence times in Yellowstone and other hot-dry rhyolites compared to cold-wet systems. Am Mineral 101:1222–1227. https://doi.org/10.2138/am-2016-5591

Lutsko JF, Maes D (2023) Simulation studies of the combined effect of mass transport and impurities on step growth. J Cryst Growth 602:126956. https://doi.org/10.1016/j.jcrysgro.2022.126956

Lutsko JF, Van Driessche AES, Durán-Olivencia MA, Maes D, Sleutel M (2016) Step crowding effects dampen the stochasticity of crystal growth kinetics. Phys Rev Lett 116:015501. https://doi.org/10.1103/PhysRevLett.116.015501

Mattinson JM, Graubard CM, Parkinson DL (1996) Oscillatory Zoning and Sub-Micron Transport of Pb. Earth processes: reading the isotopic code, 95, 355

Melnik OE, Bindeman IN (2018) Modeling of trace elemental zoning patterns in accessory minerals with emphasis on the origin of micrometer-scale oscillatory zoning in Zircon. Am Mineral 103:355–368. https://doi.org/10.2138/am-2018-6182

Peppard BT, Steele IM, Davis AM, Wallace PJ, Anderson AT (2001) Zoned quartz phenocrysts from the rhyolitic bishop tuff. Am Mineral 86:1034–1052. https://doi.org/10.2138/am-2001-8-910

Peterman EM, Reddy SM, Saxey DW, Fougerouse D, Snoeyenbos DR, Rickard WDA (2019) Nanoscale processes of trace element mobility in metamorphosed Zircon. Contrib Mineral Petrol 174:29. https://doi.org/10.1007/s00410-019-1631-1

Peterman EM, Reddy SM, Saxey DW, SnoeyenbosDR, Rickard WD, Fougerouse D, Kylander-Clark AR (2016) Nanogeochronology ofdiscordant zircon measured by atom probe microscopy of Pb-enriched dislocation loops.Science advances 2(9):e1601318.

Phelps PR, Lee CTA, Morton DM (2020) Episodes offast crystal growth in pegmatites. Nature communications, 11(1):4986.

Piazolo S, Belousova E, La Fontaine A, Corcoran C, Cairney JM (2017) Trace element homogeneity from micron-to atomic scale: implication for the suitability of the Zircon GJ-1 as a trace element reference material. Chem Geol 456:10–18. https://doi.org/10.1016/j.chemgeo.2017.03.001

Pina CM, Putnis A, Astilleros JM (2004) The growth mechanisms of solid solutions crystallising from aqueous solutions. Chem Geol 204:145–161. https://doi.org/10.1016/j.chemgeo.2003.12.002

Putnis A, Fernandez-Diaz L, Prieto M (1992) Experimentally produced oscillatory zoning in the (Ba, Sr)SO4 solid solution. Nature 358:743–745. https://doi.org/10.1038/358743a0

Ranganathan M, Weeks JD (2013) Theory of impurity induced step pinning and recovery in crystal growth from solutions. Phys Rev Lett 110:055503. https://doi.org/10.1103/PhysRevLett.110.055503

Reddy SM, Saxey DW, Rickard WD, Fougerouse D, Montalvo SD, Verberne R, Van Riessen A (2020) Atom probe tomography: development and application to the geosciences. Geostand Geoanal Res 44:5–50. https://doi.org/10.1111/ggr.12313

Remond GF, Chapoulie R, Ohnenstetter D, Roques-Carmes C, Schvoerer M (1992) Cathodoluminescence applied to the microcharacterization of mineral materials: a present status in experimentation and interpretation. Scanning Microsc 6:23–68

Rickard WD, Reddy SM, Saxey DW, Fougerouse D, Timms NE, Daly L, Jourdan F (2020) Novel applications of FIB-SEM-based ToF-SIMS in atom probe tomography workflows. Microsc Microanal 26:750–757. https://doi.org/10.1017/S1431927620000136

Sato M, Uwaha M (2001) Growth law of step bunches induced by the Ehrlich–Schwoebel effect in growth. Surf Sci 493:494–498. https://doi.org/10.1016/S0039-6028(01)01258-4

Schaltegger U, Nowak A, Ulianov A, Fisher CM, Gerdes A, Spikings R, Whitehouse MJ, Bindeman I, Hanchar JM, Duff J, Vervoort JD, Sheldrake T, Caricchi L, Brack P, Müntener O (2019) Zircon petrochronology and 40Ar/39Ar thermochronology of the Adamello intrusive suite, N. Italy: monitoring the growth and decay of an incrementally assembled magmatic system. J Petrol 60:701–722. https://doi.org/10.1093/petrology/egz010

Shore M, Fowler AD (1996) Oscillatory zoning in minerals: a common phenomenon. Can Mineral 34:1111–1126

Sleutel M, Lutsko J, Van Driessche AES (2018) Mineral growth beyond the limits of impurity poisoning. Cryst Growth Des 18:171–178. https://doi.org/10.1021/acs.cgd.7b01057

Sunagawa I (1981) Characteristics of crystal growth in nature as seen from the morphology of mineral crystals. Bull Minéral 104:81–87

Sunagawa I (2007) Crystals: Growth, Morphology, and perfection. Cambridge University Press. https://doi.org/10.1017/CBO9780511610349

Thomas TN, Land TA, Casey WH, De Yoreo JJ (2004a) Emergence of supersteps on KH2PO4 crystal surfaces. Phys Rev Lett 92:216103. https://doi.org/10.1103/PhysRevLett.92.216103

Thomas TN, Land TA, Johnson M, Casey WH (2004b) Molecular properties of adsorbates that affect the growth kinetics of Archerite (KDP). J Colloid Interface Sci 280:18–26. https://doi.org/10.1016/j.jcis.2004.07.015

Torii H, Miura H (2024) Oscillatory zoning of minerals as a fingerprint of impurity-mediated growth. Sci Rep 14:13337. https://doi.org/10.1038/s41598-024-63722-4

Valley JW, Cavosie AJ, Ushikubo T, Reinhard DA, Lawrence DF, Larson DJ, Spicuzza MJ (2014) Hadean age for a post-magma-ocean Zircon confirmed by atom-probe tomography. Nat Geosci 7:219–223. https://doi.org/10.1038/ngeo2075

Watson EB (1996) Surface enrichment and trace-element uptake during crystal growth. Geochim Cosmochim Acta 60:5013–5020. https://doi.org/10.1016/S0016-7037(96)00299-2

Wiggers de Vries DF, Bulanova GP, De Corte K, Pearson DG, Craven JA, Davies GR (2013) Micron-scale coupled carbon isotope and nitrogen abundance variations in diamonds: evidence for episodic diamond formation beneath the Siberian craton. Geochim Cosmochim Acta 100:176–199. https://doi.org/10.1016/j.gca.2012.08.034

Wu YF, Fougerouse D, Evans K, Reddy SM, Saxey DW, Guagliardo P, Li JW (2019) Gold, arsenic, and copper zoning in pyrite: a record of fluid chemistry and growth kinetics. Geology 47:641–644. https://doi.org/10.1130/G46114.1

Yang W, Lin Y, Hao J, Zhang J, Hu S, Ni H (2016) Phosphorus-controlled trace element distribution in Zircon revealed by nanosims. Contrib Mineral Petrol 171:16. https://doi.org/10.1007/s00410-016-1242-z